

RESEARCH ARTICLE OPEN ACCESS

A Biogeochemical Study of Greenhouse Gas Formation From Two Ice Complexes of Batagay Megaslump, East Siberia

Hansu Park¹  | Na-Yeon Ko¹ | JeongEun Kim¹ | Thomas Opel²  | Hanno Meyer² | Sebastian Wetterich³  | Alexander Fedorov⁴ | Andrei G. Shepelev⁴  | Hyejung Jung⁵ | Jinho Ahn¹ 

¹School of Earth and Environmental Science, Seoul National University, Seoul, Korea | ²Alfred Wegener Institute, Helmholtz Centre for Polar and Marine Research, Potsdam, Germany | ³Institute of Geography, Technische Universität Dresden, Dresden, Germany | ⁴Melnikov Permafrost Institute, Siberian Branch RAS, Novosibirsk, Russia | ⁵Department of Science Education, Ewha Womans University, Seoul, Korea

Correspondence: Jinho Ahn (jinhoahn@snu.ac.kr)

Received: 7 August 2023 | **Revised:** 10 April 2024 | **Accepted:** 6 May 2024

Funding: This study is supported by National Research Foundation of Korea (2020M1A5A1110607; 2018R1A5A1024958) grant to JA and the Leverhulme Trust Research Project Grant (RPG-2020-334) to TO.

Keywords: Batagay megaslump | biogeochemistry | greenhouse gas | ice wedge | Northeastern Siberia | permafrost

ABSTRACT

Rapidly changing permafrost landscapes are a potential key terrestrial source of greenhouse gases (GHGs) at a global scale, yet, remain poorly characterized regarding GHG origins and environmental controls on emissions. Subsurface ice wedges, commonly found across many permafrost landscapes, harbor GHG-rich gas bubbles. Analyzing these bubbles aids comprehension of subzero temperature GHG formation in permafrost. The Batagay megaslump, Earth's largest known thaw slump in northern Yakutia, provides an opportunity to study mixing ratios and isotopic compositions of both GHGs and non-GHG in ice wedge samples from two stratigraphic units: the Upper Ice Complex (UIC) and the Lower Ice Complex (LIC). The Ar/N₂/O₂ compositions and bubble shapes indicated that the studied ice wedges were likely formed through dry snow and/or hoarfrost compaction, and microbial activity remained active after ice wedge formation. The high CO₂ and CH₄ mixing ratios and carbon stable isotope values suggested that CO₂ and CH₄ primarily originated from microbial sources. N₂O showed an “exclusive relation” with CH₄—meaning that high N₂O is observed only when CH₄ is low, and vice versa—and N₂O mixing ratios vary at different depths. These findings suggest that GHG formation in ice wedges is not solely controlled by physiochemical conditions, but involves a complex interplay between microbial activity and environmental conditions. Our study contributes to a better understanding of the dynamics involved in GHG formation within degrading permafrost landscapes.

1 | Introduction

In the current global warming crisis, the rapid increase in greenhouse gas (GHG) in the atmosphere is of great concern. Permafrost contains a large reservoir of organic carbon and nitrogen in terrestrial regions and multiple lines of evidence show that permafrost may emit a significant amount of GHGs into the atmosphere up on thawing, thus accelerating global warming

[1–3]. Yedoma, found in East Siberia and Alaska, refers to Late Pleistocene organic and ice-rich silty permafrost deposits containing large ice wedges, which are characterized by higher ice content compared with other permafrost sediments, making it particularly vulnerable to the impact of climate change [4, 5]. The Intergovernmental Panel on Climate Change (IPCC) reported that permafrost regions are more sensitive to global warming owing to their high latitudinal location; hence, GHG

This is an open access article under the terms of the [Creative Commons Attribution-NonCommercial](https://creativecommons.org/licenses/by-nc/4.0/) License, which permits use, distribution and reproduction in any medium, provided the original work is properly cited and is not used for commercial purposes.

© 2024 The Authors. *Permafrost and Periglacial Processes* published by John Wiley & Sons Ltd.

formation from Yedoma deposits is a key factor affecting further GHG emissions [6].

Ice wedges are characteristic of permafrost regions, and are formed when thermal contraction cracks appear in the ground during winter [7]. The cracks are filled via two main processes: meltwater refreezing in spring and snow/hoarfrost accretion in-filling [8]. Additionally, sediment and soils from the land surface or the active layer can enter frost cracks with water or snow and produce foliation in ice wedges. Soils combined with water and snow may facilitate microbial activities related to GHG formation. Although GHG emissions from permafrost soils have been investigated comprehensively [9–11], previous studies pertaining to ice wedges have primarily focused on winter climate reconstructions and stable water isotope analysis [12]. Meanwhile, studies that directly measure the mixing ratios of GHGs and the compositions of other gases within ground ice and ice wedges are rare [13–15].

Investigations pertaining to ice wedges in Alaska and Siberia, particularly in Yakutia, have progressed, with emphasis on the analysis of ice wedges in lowland areas near rivers or coastlines [13]. However, ice wedges in continental highlands are rarely investigated. The Batagay megaslump is located in the Yana Highlands, which are characterized by some of the most extreme continental climate conditions in the Northern Hemisphere [16]. The exposure of the Batagay megaslump provides valuable data pertaining to GHGs within the ice wedges formed under continental conditions. This megaslump has experienced rapid thawing and significant growth in the past, with a thermo-denudation rate of 15 m/year. As of 2019, the maximum width of the slump was 890 m [17]. In the Batagay megaslump, there are 7 stratigraphic units exposed. Our study focuses on two ice complex units, namely the Upper Ice Complex and the Lower Ice Complex. Henceforth, we will use the abbreviations UIC and LIC for these ice complexes.

These ice complexes reveal the presence of ice wedges that formed during the Middle and Late Pleistocene [18]. The Batagay megaslump has revealed ancient syngenetic permafrost, which

formed simultaneously with the ongoing sedimentation in cold climates. The stratigraphy of the Batagay megaslump implies that the gas bubbles and sediments trapped within the ice wedges may contain valuable information about the environmental conditions during their formation in the Middle and Late Pleistocene [18, 19]. Additionally, ice wedges serve as a sanctuary for diverse and active microbial communities in cold permafrost regions, and the presence of active microorganisms contributes to the formation of GHGs [20].

In this study, we analyze the gas in bubbles entrapped in ice wedges from two ice complex units of the Batagay megaslump, along with sediment and stable water isotope chemistries to unravel the potential influence of biogeochemical and environmental factors on the GHG formation within ice wedges. The potential of GHG formation and emission potentials from permafrost of the Batagay megaslump could be significant, due to the high wedge-ice volume in both ice-oversaturated ice complex deposits; amounting up to 70% by volume in the UIC and 56% by volume in the LIC [21].

The specific objectives of this study are (1) to propose a possible formation process for the ice wedges based on air composition ($\text{Ar}/\text{N}_2/\text{O}_2$) and stable water isotopes to predict the occurring gas-forming reactions in a stable system and under climatic conditions during formation, and (2) to propose possible biogeochemical processes of GHG formation for both ice complex units under subfreezing temperatures. Achieving these objectives will lead to a deeper comprehension of the process of GHG formation and potential GHG emissions from permafrost areas.

2 | Site and Sample Description

Ice-wedge samples were obtained from the Batagay megaslump (67.58°N, 134.77°E) in north-eastern Siberia, Russia, in March to April of 2019 (Figure 1). The Batagay megaslump is located near the village of Batagay on the east bank of the Yana River in the Yana Highlands. It is situated on a hillslope

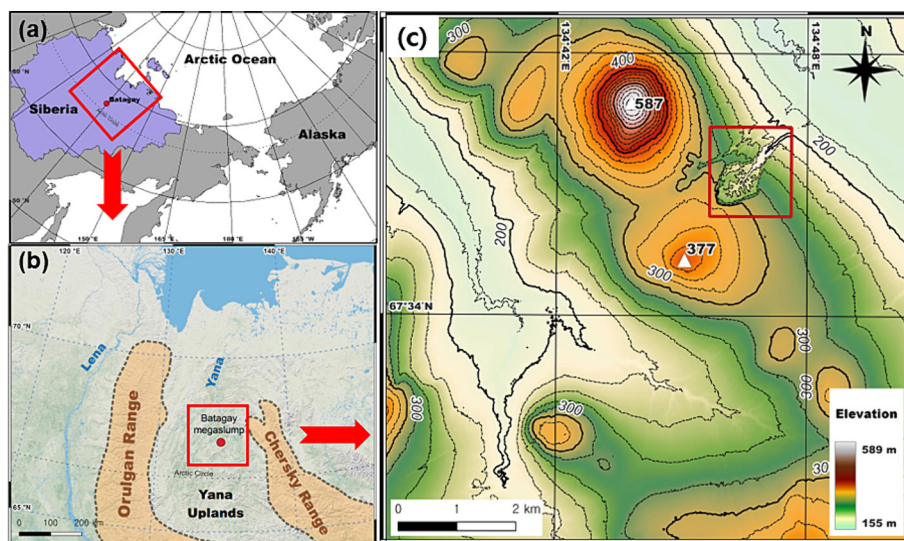


FIGURE 1 | (a) Location map of Batagay and the Arctic Ocean. Red box indicates location of panel (b). (b) Location map showing Batagay megaslump within the Yana River basin in northern Yakutia. Shaded and dashed orange lines depict two mountain ranges surrounding the Yana Uplands. Red box indicates location of panel (c). (c) Topographic map of Batagay megaslump (red box), illustrating its position on a northeast-facing hillslope.

at an elevation of approximately 290 m above sea level and is the world's largest known thaw slump [16, 17, 22]. The region is characterized by a strong continental climate, with increasing temperature and precipitation trends since the mid-20th century [17]. The permafrost is continuous and 200–500 m thick, and the active layer is 0.2–1.2 m thick. The vegetation near Batagay mainly comprises open woodlands dominated by Dahurian larch (*Larix gmelinii* (Rupr.)) with dwarf birch (*Betula nana* subsp. *exilis*(L.)) understorey and ground cover consisting of lichens and mosses [17].

The Batagay megaslump exposes Middle and Late Pleistocene to Holocene permafrost formations spanning from at least Marine Isotope Stage (MIS) 16 to 1 [18]. Previous studies have identified seven main stratigraphic units in the area [16, 18, 22, 23]. The lowest unit comprises clasts-supported diamicton. The LIC (Lower Ice Complex, MIS 16) above includes V-shaped ice wedges that are 2–3 m high and approximately 1 m wide at the top, and are truncated by thaw unconformities. An overlying lower sand unit (~MIS 7 to 4) is approximately 20 m thick and composed of yellowish pore ice-cemented sand with gray horizontal bands. It contains narrow syngenetic ice wedges up to 0.5 m wide. The UIC (Upper Ice Complex, MIS 4 to 3), which is 20–25 m thick, is dominated by large syngenetic ice wedges [22].

For our study, we examined three samples from three ice wedges from the LIC and ten samples from four ice wedges of the UIC (Figure 2). In the LIC, the ice wedge samples were labeled as B19-IW1-gas, B19-IW3-gas, B19-IW5-gas, while in the case of UIC, as B19-IW8-gas1, 2; B19-IW9-gas1, 2, 3, 4; B19-IW10-gas1, 2; and B19-IW11-gas1, 2. The samples were cut from the

ice wedges with a chain saw as huge blocks (approximate size 25x15x15 cm) and kept frozen until laboratory analyses.

3 | Materials and Methods

3.1 | Gas Extraction and Mixing Ratio Measurements

Dry and wet (melt–refreeze) extraction methods were used to extract the gas enclosed in the ice wedge samples. Both methods have the same purpose; however, wet extraction is predominantly used owing to its high air yield. Both extraction systems were employed at the SNU (Seoul National University) [13, 25]. The details of the extraction systems have been compared comprehensively by Yang et al. [26].

We collected three ice blocks from the LIC and ten blocks from the UIC for subsequent gas analysis. For every block, we extracted gas from three to six subsamples (7 cm × 3 cm × 3 cm). A total of 22 subsamples were extracted using the dry extraction method and 33 subsamples were analyzed via the wet extraction. Ice wedge subsamples were mainly cut with a band saw, but for particularly hard ice, we also used a hand saw and a hammer.

For the dry extraction method, 33 g of ice was used, and because the system could only measure a maximum of 12 g of ice simultaneously, we conducted three separate attempts to obtain data for one subsample. Each ice sample was placed inside the vacuum chamber, and needle were used to crush the ice. To remove water vapor, we used a cold trap with ethanol at -85°C .

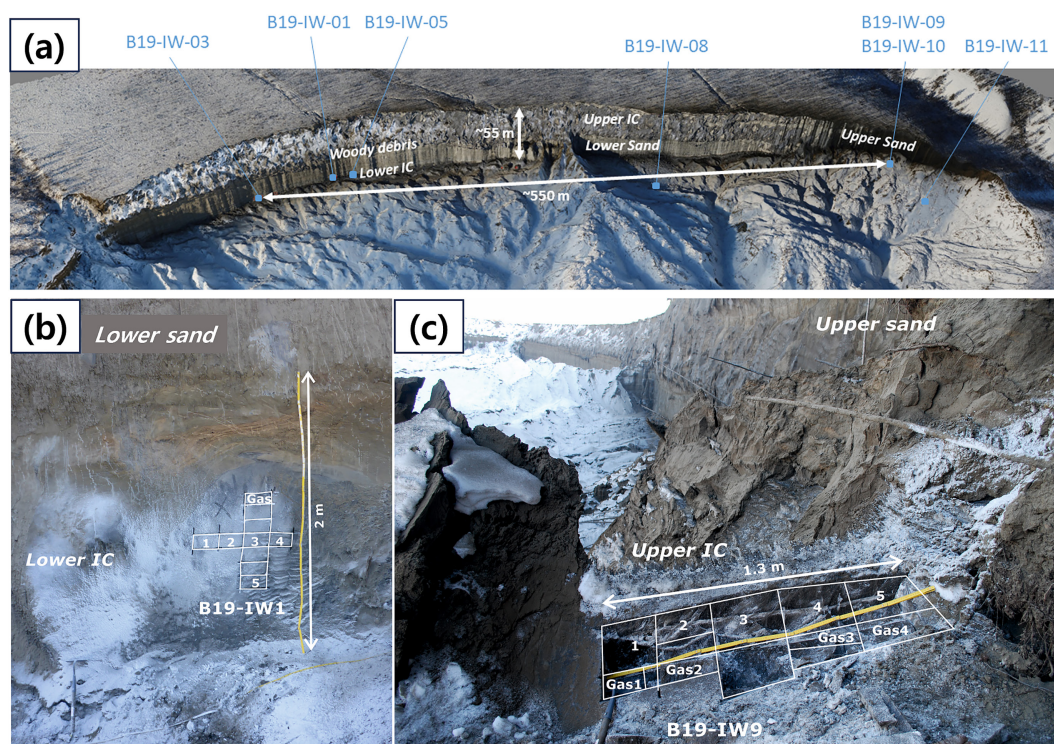


FIGURE 2 | (a) Headwall of the Batagay megaslump with approximate sampling positions. (b) Ice wedge B19-IW1 from the Lower Ice Complex with sample locations. (c) Ice wedge B19-IW9 from the Upper Ice Complex with sample locations. The images are modified from Batagay field report in 2019 [24].

For the wet extraction, we placed 50g of ice in a glass bottle. Each ice sample was melted to extract gas and then refrozen to increase the extraction efficiency and remove water vapor by soaking the glass bottles in an ethanol bath at -70°C for approximately 20 min. Afterwards, we preserved the ice melt and sediment mixtures in high density polyethylene (HDPE) bottles and stored them in a freezer at -20°C for later use.

For both extraction systems, the gas extracted from the ice wedges was trapped at -256°C using a He closed-cycle refrigerator, which effectively cryogenically preserved the gas in a stainless-steel tube. After trapping, the sample tubes were sealed, heated to room temperature, and separated into two tubes for measuring air composition ($\text{Ar}/\text{O}_2/\text{N}_2$) and greenhouse gas mixing ratios (CO_2 , CH_4 , and N_2O). Because the dry extraction method shows lower gas yield than the wet extraction method, only greenhouse gas mixing ratios of the gas extracted from dry extraction could be measured, while both air composition and greenhouse gas mixing ratios could be measured from the wet-extracted gas. There was little difference in results of greenhouse gas concentrations between the two extraction methods, confirming a previous methodological study [25].

The gas mixing ratios were measured simultaneously using three gas chromatography (GC) systems. An Agilent 7890A GC system equipped with a flame ionization detector (FID) and a catalyst methanizer was employed to measure CO_2 mixing ratios. The N_2O and CH_4 concentrations were measured using an Agilent 7890B GC system equipped with an electron capture detector and FID. To measure the mixing ratios of Ar, O_2 , and N_2 , a 7890A GC system equipped with a FID/TCD was utilized. The $\delta(\text{N}_2/\text{Ar})$ and $\delta(\text{O}_2/\text{Ar})$ values were expressed as percentages (%) of the present-day molar atmospheric ratio using the following equation, where X represents N_2 or O_2 :

$$\delta\left(\frac{X}{\text{Ar}}\right) = \left[\frac{\left(\frac{X}{\text{Ar}}\right)_{\text{sample}}}{\left(\frac{X}{\text{Ar}}\right)_{\text{air}}} - 1 \right] \times 100 (\%)$$

The $\delta(\text{N}_2/\text{Ar})$ molar ratios or other noble gas ratios can be used to elucidate the formation process of ice wedges and as indicators of gas alteration during or after ice wedge formation. N_2 and other noble gases are not significantly affected by biological activity and exhibit different solubility in water, and therefore if ice wedges have undergone physical re-working processes, such as melt-refreezing or formation from liquid water, then the $\delta(\text{N}_2/\text{Ar})$ value is likely to be below 0 and potentially close to -55.5% . This is based on the assumption that atmospheric gases equilibrate with water at the freezing point and that the gas composition remains unchanged during freezing. By contrast, if ice is formed through snow compaction or have not undergone melt-refreezing, then the $\delta(\text{N}_2/\text{Ar})$ value should be approximately 0% [8].

The $\delta(\text{O}_2/\text{Ar})$ ratio can serve as an indicator of biological activity. An absence of biological activities in the ice wedges would result in $\delta(\text{O}_2/\text{Ar})$ to be approximately 0%. However, a $\delta(\text{O}_2/\text{Ar})$ value below 0 suggests the presence of oxygen consuming microbiological activity [8]. Since during the Quaternary, the atmospheric molar ratios of N_2/Ar and O_2/Ar

remained nearly constant [27]. Consequently, the changes in these values can serve as indicators of gas alteration during or after ice wedge formation.

3.2 | Stable Water Isotope Analysis

Stable water isotope composition analysis ($\delta^{18}\text{O}$ and δD) for the ice wedges was conducted using meltwater that remained after the wet extraction process. The meltwater samples were centrifuged and filtered to remove organic matter and microparticles using a $0.45\ \mu\text{m}$ syringe filter. The filtered samples were placed inside PVC bottles and stored in a freezer at -20°C until stable isotope analysis was performed. The stable water isotopic compositions were analyzed at Ewha Womans University, Korea, using an L2140-i model isotopic water liquid analyzer (Picarro Inc., Sunnyvale, CA, USA) based on the wavelength-scanned cavity ring-down spectroscopy method. The standards were Vienna Standard Mean Ocean Water 2 (VSMOW2), Standard Light Antarctic Precipitation (SLAP), USGS 46, 47, and 48, whose mean standard deviations were less than 0.1‰ for $\delta^{18}\text{O}_{\text{ice}}$ and less than 1.0‰ for δD . A total of 11 and 29 samples were obtained from the LIC and UIC, respectively. The isotopic ratios were expressed in per mill (‰) relative to the standard mean ocean water (SMOW) using the following equation: $R = {}^{18}\text{O}/{}^{16}\text{O}$ or D/H .

$$\delta_{\text{Sample}} = \left(\frac{R_{\text{Sample}}}{R_{\text{Standard}}} - 1 \right) \times 1000 (\text{‰})$$

We also calculated deuterium excess (d-excess) as a key metric to characterize the isotopic composition of our ice samples. This parameter is defined as the difference between the δD and $\delta^{18}\text{O}_{\text{ice}}$, expressed by the following equation: [28]

$$\text{Deuterium excess (d - excess)} = \delta\text{D} - 8 \times \delta^{18}\text{O}_{\text{ice}}$$

The water stable isotopes (δD and $\delta^{18}\text{O}_{\text{ice}}$) and deuterium excess provide valuable insights into the circumstances influencing the formation of ice and contribute to the identification of moisture sources.

3.3 | Sediment and Major Ion Chemistry

To analyze the sediment and major ion chemistry, we obtained 3 mL of filtered water and stored it in HDPE bottles. The analysis of major ions aimed to identify potential ion-related biotic reactions leading to greenhouse gas formation. Both anions (Cl^- , NO_3^- , NO_2^- , and SO_4^{2-}) and cations (NH_4^+ , Ca^{2+} , Mg^{2+} , Na^+ , and K^+) were analyzed using an ion chromatograph at the National Instrumentation Center for Environmental Management (NICEM, Seoul National University, Seoul, Republic of Korea). For total Fe concentration, we analyzed 10 mL of filtered water using an Inductively Coupled Plasma-Mass Spectrometry (ICP-MS) at the NICEM. The measurement units for all ions, excluding Fe, were in the mg/L range, while Fe concentrations were measured at the $\mu\text{g}/\text{L}$ level.

In order to ascertain the origin of greenhouse gases, we analyzed the content (C and N) and the respective isotopic composition ($\delta^{13}\text{C}$ and $\delta^{15}\text{N}$) of sediment entrapped within ice wedges. We separated the sediment samples and dried them under ambient

conditions for 48 h. After the sediments were completely dried, we used Midwood and Boutton's (1998) method to remove carbonate minerals [29]. For the removal, we performed the following steps: 0.3 g sediment for each sample was soaked in 0.5 M HCl solution. The sediment–HCl solution was maintained at 24 h and stirred thrice during the reaction. Subsequently, they were separated via centrifugation at 4000 RPM for 7 min. Next, the samples were washed with deionized water four times via the same centrifugation process. Meanwhile, the sediments were dried at 87°C for 24 h, stored in a 1.5 mL conical tube, and sent to NICEM (National Instrumentation Center for Environmental Management) at SNU for the analyses of $\delta^{13}\text{C}$, $\delta^{15}\text{N}$, total carbon, and total nitrogen in sediments.

3.4 | Stable Carbon Isotopes for Greenhouse Gas

We determined the carbon isotope ratios of CO_2 and CH_4 gases to assist in source attribution. The wet extraction method was used to extract CO_2 and CH_4 , which were then stored in stainless-steel tubes for subsequent analysis. The $\delta^{13}\text{C}\text{-CO}_2$ and $\delta^{13}\text{C}\text{-CH}_4$ values were measured at Nagoya University, Japan, using a CF-IRMS system [30–32]. Three samples from both the LIC and UIC were analyzed for $\delta^{13}\text{C}\text{-CO}_2$, whereas one sample from the LIC and two samples from the UIC were measured for $\delta^{13}\text{C}\text{-CH}_4$. The standard deviation was 0.1‰–0.2‰ for $\delta^{13}\text{C}\text{-CO}_2$ and <0.2‰ for $\delta^{13}\text{C}\text{-CH}_4$.

3.5 | Observation of Bubble Shapes

To examine physical changes in ice wedges, thin sections were made to observe bubble shapes inside the ice wedges. Two section samples were obtained from UIC, and one from LIC. The ice

wedge samples were cut to a thickness of 2 mm, and the surfaces were smoothed using sandpaper (Figure S1).

4 | Results

4.1 | Stable Water Isotopes

The $\delta^{18}\text{O}$ and δD values of the LIC ranged from -32.82‰ to -30.58‰ and -251.04‰ to -234.65‰ respectively. The UIC showed more depleted values of $\delta^{18}\text{O}$ and δD than the LIC, which ranged from -36.63‰ to -33.05‰ and -284.74‰ to -259.30‰ , respectively (Table 1, S3, Figure 3). The deuterium excess (d-excess) values of the LIC and UIC were 7.72‰ to 18.14‰ and 4.64‰ to 10.96‰, respectively. The linear regression between $\delta^{18}\text{O}$ and δD yielded equations of $\delta\text{D} = 7.32 \times \delta^{18}\text{O} - 15.75$ and $\delta\text{D} = 9.31 \times \delta^{18}\text{O} + 54.24$ for the LIC and UIC, respectively.

4.2 | N_2 , O_2 , and Ar Mixing Ratios

Our measurements of $\delta(\text{N}_2/\text{Ar})$ in the Batagay ice wedges ranged from -8.06% to 33.86% for the LIC and from 5.49% to 30.64% for the UIC (Figure 4, Table S1). The $\delta(\text{O}_2/\text{Ar})$ values ranged from -89.01% to -67.43% and -98.07% to -47.06% for the LIC and UIC, respectively.

4.3 | Greenhouse Gas Mixing Ratios

The mean CO_2 , CH_4 , and N_2O mixing ratios and their standard deviation (1σ) of the Batagay ice wedge for the LIC were $3.88 \pm 2.14\%$ (CO_2), 90.08 ± 47.51 ppm (CH_4), and 1.16 ± 2.05 ppm (N_2O), and for the UIC $3.90 \pm 2.23\%$ (CO_2),

TABLE 1 | Mean, maximum, and minimum values of gas composition (CO_2 , CH_4 , N_2O , Ar, O_2 , and N_2), air contents, water stable isotopes, sediment contents, and sediment chemistry for LIC and UIC layers.

Parameter	Lower Ice Complex (B19-IW1, 3, 5)				Upper Ice Complex (B19-IW8, 9, 10, 11)			
	Mean	Max.	Min.	n	Mean	Max.	Min.	n
Ar (%)	0.95	1.04	0.76	9	1.07	1.20	0.87	26
O_2 (%)	4.45	7.50	2.49	9	3.97	12.85	83.48	26
N_2 (%)	89.63	95.18	79.30	9	92.00	98.77	83.48	26
N_2O (ppm)	1.16	8.16	0.12	14	19.45	111.88	0.30	38
CH_4 (ppm)	90.08	182.04	31.17	14	54.97	136.42	4.76	38
CO_2 (%)	3.88	10.30	1.88	15	3.90	7.82	0.03	38
Gas contents (mL/g _{ice})	0.0101	0.0193	0.0034	10	0.0110	0.0218	0.0028	25
$\delta^{18}\text{O}_{\text{ice}}$ (‰)	-32.02	-30.58	-32.82	11	-34.67	-33.05	-36.63	29
$\delta\text{D}_{\text{ice}}$ (‰)	-243.87	-234.65	-253.75	11	-269.46	-259.30	-284.74	29
d-excess(‰)	12.27	18.14	7.22	11	7.87	10.96	4.64	29
Sediment contents (g/g _{ice})	0.0136	0.0171	0.0083	4	0.0179	0.0592	0.0051	11
Sediment C (wt%)	0.74	0.99	0.54	5	1.17	1.52	1.00	5
Sediment N (wt%)	0.07	0.10	0.06	5	0.12	0.16	0.09	5
Sediment $\delta^{13}\text{C}$	-25.80	-25.74	-25.96	5	-25.56	-25.36	-25.97	5
Sediment $\delta^{15}\text{N}$	3.38	6.77	0.92	5	4.10	9.14	2.40	5
C/N	9.76	11.23	8.42	5	10.19	11.42	9.40	5

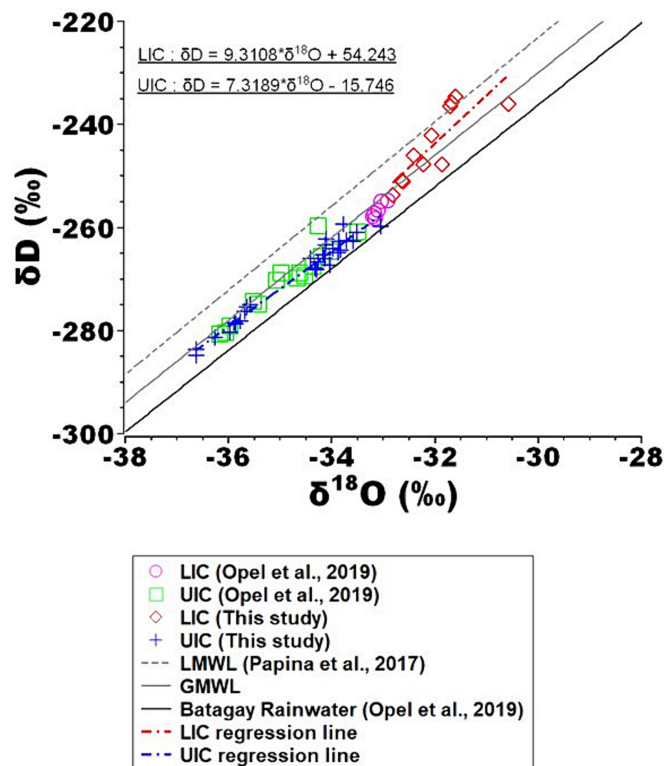


FIGURE 3 | Dual water stable isotope diagram for Batagay ice wedges. Global Meteoric Water Line (GMWL) is indicated by $\delta D = 8 \times \delta^{18}O + 10$ and Local Meteoric Water Line (LMWL for Yakutsk, 600 km south of Batagay) is indicated by $\delta D = 8.17 \times \delta^{18}O + -21.94$, based on Papina et al. [33] Batagay rainwater ($n = 4$) is indicated by $\delta D = 7.93 \times \delta^{18}O - 1.65$ based on Opel et al. [22] Dash-dotted red and blue lines are regression lines for LIC and UIC, respectively.

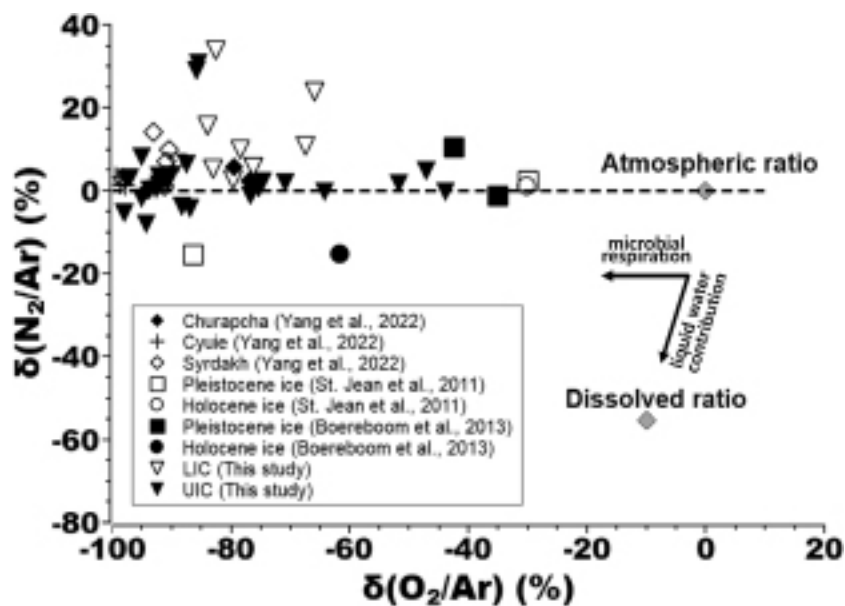


FIGURE 4 | $\delta(N_2/Ar)$ and $\delta(O_2/Ar)$ mixing ratios of various ice wedges corresponding to different locations and ages. Shaded gray and outlined black diamonds reflect atmospheric ratio or each gas completely dissolved in liquid water, respectively. Unfilled or filled lower triangles indicate Batagay LIC and UIC, respectively. Other symbols represent ice wedge values in the Yakutsk region in Central Siberia formed during the Last Glacial Period [15], those near the Laptev Sea region formed in the late Pleistocene and Holocene [14], and those in the Alaska region formed in the Pleistocene and Holocene [8].

54.97 ± 24.94 ppm (CH_4), 19.45 ± 25.30 ppm (N_2O), respectively (Table 1, S1, Figure 5). The relationship between the GHG mixing ratios in the Batagay ice wedges did not indicate any

significant correlations ($|r| < 0.24$). However, it is clear that N_2O is high only when CH_4 is low, and vice versa (Figures 5, 6 and Table S6). We also observed a similar “exclusive relation”

between the N_2O and CH_4 mixing ratios in the previous study at Yakutsk area (Yang et al., 2022, Figure 7). When compared with ice wedges in other Siberian regions, specifically those located in the interior of Yakutia, such as Churapcha, Cyuie, and Syrdakh, the Batagay ice wedges generally exhibited low CO_2 but high N_2O and CH_4 levels (Figure 7) [13, 15]. Finally, there was a weak negative correlation ($r = -0.54$) between CO_2 and CH_4 .

4.4 | Sediment and Ion Properties

The mean sediment contents (1σ) of the LIC and UIC ice wedge samples were 0.0136 ± 0.0038 and 0.0179 ± 0.0158 g/ g_{ice} , respectively (where g_{ice} is the unit weight of an ice and sediment mixture from an ice wedge). The mean carbon and nitrogen ratios, C/N (1σ) for the LIC and UIC were 9.76 ± 1.18 and 10.19 ± 0.84 , respectively; their mean $\delta^{13}C$ values (1σ) were $-25.80 \pm 0.09\%$ and $-25.56 \pm 0.24\%$; and their mean $\delta^{15}N$ values (1σ) were $3.38 \pm 2.23\%$ and $4.10 \pm 0.24\%$, respectively (Tables 1 and S5).

Ion and Fe concentrations in the meltwater samples from LIC and UIC are shown in Table S2. In particular, NO_3^- concentrations were 9.21 mg/L ($n=1$) and 10.13 ± 0.15 mg/L ($n=2$) for the LIC and UIC, respectively. NH_4^+ concentrations were 2.25 ± 1.42 mg/L ($n=5$) and 2.13 ± 1.08 mg/L ($n=4$) mg/L for the LIC and UIC, respectively. It should be noted that NO_2^- concentrations were only measured in the UIC samples, and the concentration was 1.58 ± 1.44 mg/L ($n=3$). The LIC samples either were not measured or fell below the detection limit for NO_2^- . Additionally, the Fe concentrations were 386.11 ± 216.84 μ g/L ($n=5$) and 47.50 ± 67.82 μ g/L ($n=5$) for the LIC and UIC, respectively.

4.5 | $\delta^{13}C$ for Greenhouse Gas

The average $\delta^{13}C$ - CO_2 values for the LIC and UIC samples were determined to be $-22.8 \pm 1.80\%$ ($n=3$), $-23.8 \pm 1.43\%$ ($n=3$), respectively. These values are close to or within the range of carbon isotope values of CO_2 derived from sediment organic carbon ($\delta^{13}C = -25.8 \pm 0.09\%$, $n=5$ for LIC; $\delta^{13}C = -25.56 \pm 0.24\%$, $n=5$ for UIC) (Table S4), but very different from those of pre-industrial atmospheric CO_2 ($\delta^{13}C = -6.7\%$) [34]. Additionally, Average $\delta^{13}C$ - CH_4 values were $-48.1 \pm 1.12\%$ ($n=2$) and -36.7% ($n=1$) for the LIC and UIC, respectively (Table S4).

5 | Discussion

5.1 | Batagay Ice Wedge Formation and Related Climate Conditions

We used the gas composition and water-stable isotopes to assess ice wedge formation and the related climatic conditions. Our $\delta(N_2/Ar)$ values relative to atmospheric air were mostly 0% or higher (Figure 4). This suggests that the ice wedges were not formed by freezing of liquid snowmelt water, but rather by the compaction of dry snow or hoarfrost. The shapes of the bubbles within the ice wedges also provide information regarding their formation (Figure S1). If ice wedges were formed by refreezing of meltwater, then the bubbles generated may exhibit elongated shapes and a preferred orientation [8]. However, upon examining thin sections (~2 mm thick) of the Batagay ice wedges, we observed spherical bubbles in the both ice complexes (Figure S1). Meanwhile, upon inspecting the bulk ice blocks, we did not observe any perturbations in the foliation, thus indicating that the ice wedges were not disrupted by melting after formation.

The $\delta(N_2/Ar)$ values ranging from 10% to 20% in the Batagay ice wedges, are higher than the typically observed values of approximately or less than 0% in other Siberian ice wedges (Figure 4). To explain this elevation in the N_2/Ar values, we may consider a differential gas diffusion through the ice lattice by faster Ar diffusion than N_2 through ice. Previous studies have confirmed that gas molecules can diffuse through ice via interstitial or bond-breaking mechanisms, as supported by molecular dynamics (MD) simulations [35–38]. To quantify this effect, we employed equations for gas permeation coefficients (diffusion coefficients \times solubility) in ice. Using the parameters described by Oyabu et al. [39], we calculated the permeation coefficients for N_2 and Ar at $-10^\circ C$, and obtained 1.31×10^{-19} and 4.16×10^{-19} $m^2/s \cdot MPa$, respectively. These values indicate that the permeability of Ar is higher than that of N_2 . Consequently, the N_2/Ar ratio in both Batagay ice complex units may be increased by gas diffusion within the ice matrix. We observe that the LIC generally exhibited higher N_2/Ar values than the UIC. This difference may be caused by the fact that the LIC is located at a greater depth, experiencing higher pressures and having longer time (~650 ka for LIC vs. ~40 ka for UIC) for the differential diffusion than the UIC.

Stable water isotope ratios of ice wedge ice can be used to investigate winter temperature conditions during the ice wedge formation, with a positive correlation between the winter temperatures

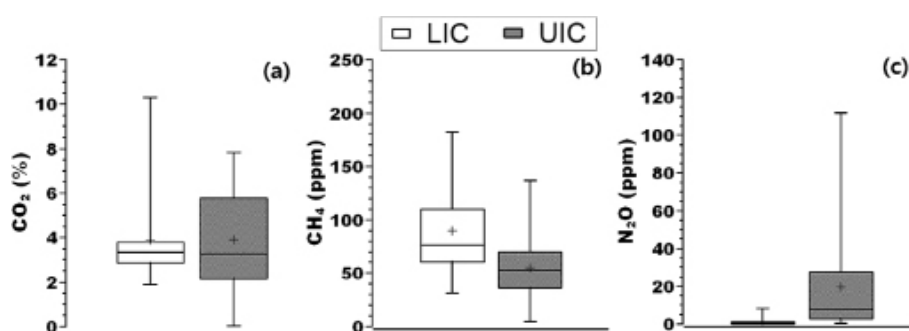


FIGURE 5 | Greenhouse gas mixing ratios in ice wedges of the Batagay megaslump. The box represents the interquartile range, with the bottom and top indicating the 25th and 75th percentiles, respectively. The horizontal line within the box represents the median value, whereas the “+” symbol denotes the mean value. Whiskers extending from each end of the box represent minimum and maximum values of the data points.

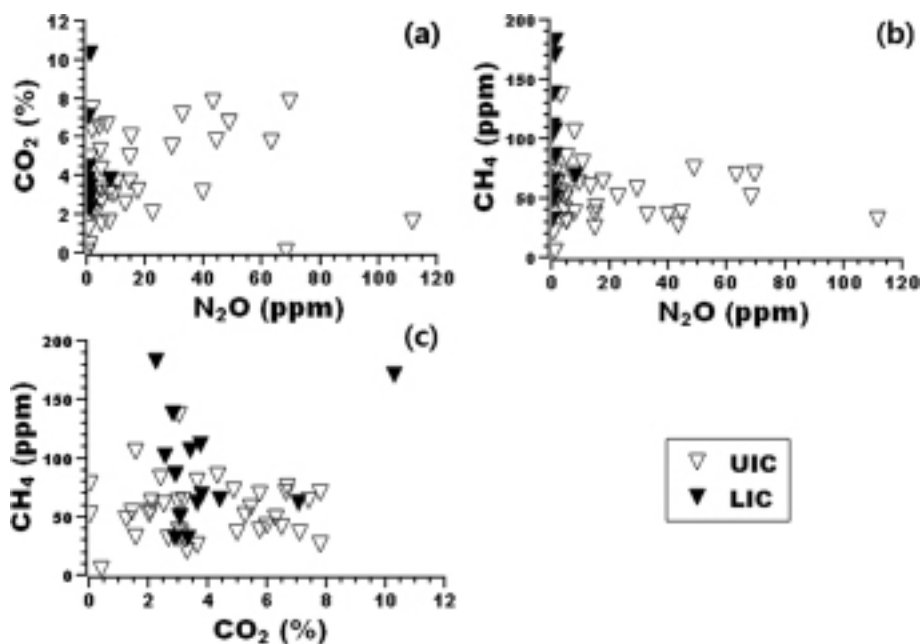


FIGURE 6 | Scatter plots of greenhouse gas mixing ratios in Batagay ice wedges for UIC and LIC units. (a) CH₄ versus CO₂, (b) N₂O versus CH₄, (c) CO₂ versus CH₄. Each gas mixing ratio was measured simultaneously in the same extracted gas at the LIC and UIC. Unfilled and filled lower triangles represent data from UIC and LIC, respectively.

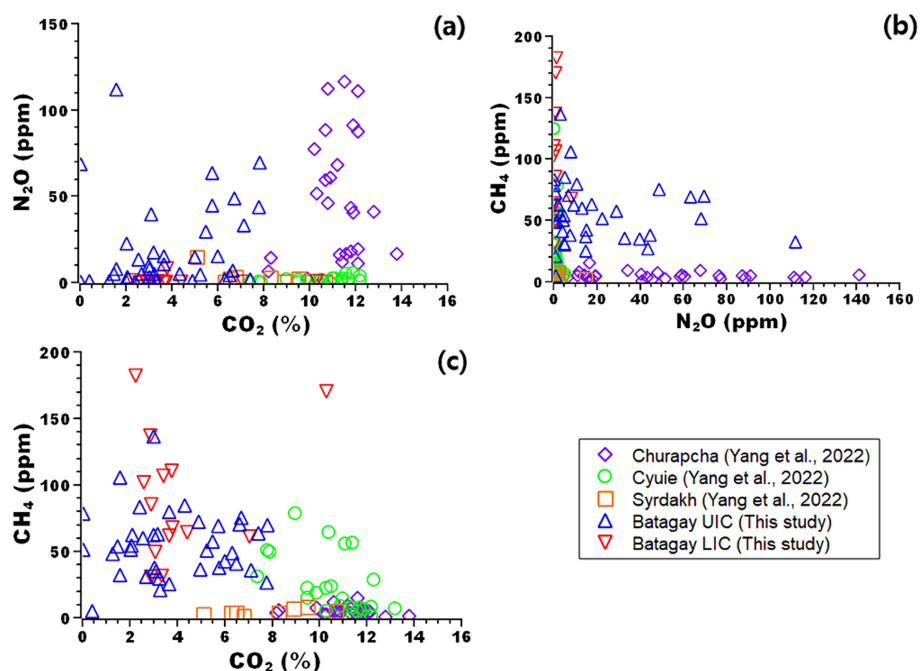


FIGURE 7 | Scatter plots of greenhouse gas relationships in ice wedges from different ages and locations in Siberia (Churapcha, Cyuie, Syrdakh, and our study site Batagay). (a) N₂O versus CO₂, (b) CH₄ versus N₂O, (c) CH₄ versus CO₂. Ice wedges data from Churapcha, Cyuie, Syrdakh were obtained from ref. [15]

and $\delta^{18}\text{O}$ values [7]. We observed that the UIC exhibited more depleted $\delta^{18}\text{O}$ values as compared with the LIC, with a difference of approximately 2.7‰ (Figure 3, Table 1). This suggests that the LIC ice wedges have formed at slightly higher winter temperatures as compared with those of the UIC, even though their isotopic composition might be altered due to their old age.

The potential effects of post-depositional isotopic fractionation must be considered for the use of ice wedges as archives

for winter temperature as the original isotopic signature of ice can be altered due to isotopic exchange between wedge ice and pore ice of the surrounding sediments [40, 41]. Our LIC samples exhibited slightly enriched $\delta^{18}\text{O}$ and δD and a steeper slope as compared with the GMWL. However, the isotopic compositions of δD and $\delta^{18}\text{O}$ in the entire Batagay megaslump ice wedges, largely aligned with the GMWL and the local meteoric water line of Yakutsk. Furthermore, the $\delta^{18}\text{O}$ values of the ice wedges generally reflected a similar trend to that reported by Opel et al.

[22] These observations suggest that the isotopic compositions are unlikely to be significantly altered.

5.2 | Origin of GHGs Within Ice Wedges

To understand the origin of GHGs entrapped in ice wedges, one must verify whether the ice wedges have been maintained in a stable state without being subjected to processes such as breakage or disruption. The Batagay megaslump ice wedges appeared to be unaltered and well-preserved under stable conditions, as indicated by the undisrupted foliation and spherical bubble shapes as well as the zero to positive values of $\delta(N_2/Ar)$ relative to the atmospheric N_2/Ar ratio. Hence, we can assume that the ice wedges from the Batagay permafrost are quasi-closed and stable systems. Meanwhile, as Batagay ice wedges are likely formed by snow and/or hoarfrost compaction, it is probable that the initial mixing ratios of GHGs are atmospheric values, and that the observed high mixing ratios of GHG in the bubbles of the Batagay ice wedges are due to the formation of GHG inside the ice wedges.

The dissolution of atmospheric GHGs (CO_2 , CH_4 , and N_2O) in liquid water can increase the mixing ratios of GHGs. If an equilibrium exists between air and snow/ice meltwater, then the GHG mixing ratios in the liquid water can increase up to 60, 2, and 45 times the atmospheric level for CO_2 , CH_4 , and N_2O , respectively [42]. Consequently, if the snowmelt-refreeze process is involved in ice wedge formation, then we can expect the GHG mixing ratios in ice wedges to be up to 16,800, 1.4, and 12.6 ppm for CO_2 , CH_4 , and N_2O , respectively [13]. However, because evidence of melting during or after ice wedge formation was not indicated, we precluded this process as the main source of GHGs in ice wedges. Notable, however, these GHG mixing ratios in gas bubbles in the Batagay ice wedges were two to three orders of magnitude greater than those of the Pleistocene atmospheric level [43–45].

Microbial activity has been shown to persist even at soil temperatures below $0^\circ C$ [46, 47]. Despite having limited substrates and energy sources for their metabolic processes, these microorganisms are crucial in maintaining high mixing ratios of GHGs in ice wedges. Bacteria can remain viable for thousands of years through active reproduction or by maintaining the minimal activity levels necessary for the repair of cellular damage. In permafrost, the necessary energy for sustaining cellular functions or facilitating reproduction can be potentially derived from material released from frozen sediments [48]. In Batagay ice wedges, the main source of nutrients might be the sediments entrapped during the ice wedge formation.

The initial main air composition (O_2 , N_2 , and Ar) during the formation of ice wedges would have been similar to that of the atmosphere [8]. However, microbial activity in the ice wedge that consumes oxygen gas (O_2) may result in oxic to anoxic or oxygen-depleted conditions. Notably, the heterogeneous distribution of the sediment content in ice wedges must be considered, as the presence or absence of O_2 can vary across different microsites in an ice wedge. Furthermore, the permeability of gas molecules can influence the mixing ratios in ice bubbles. O_2 and Ar have higher permeability coefficients (4.16×10^{-19} and $3.39 \times 10^{-19} \text{ m}^2/\text{s} \cdot \text{MPa}$, respectively) than N_2 ($1.31 \times 10^{-19} \text{ m}^2/\text{s} \cdot \text{MPa}$) and other major greenhouse

gases (CO_2 : 1.39×10^{-19} and CH_4 : $7.08 \times 10^{-20} \text{ m}^2/\text{s} \cdot \text{MPa}$, N_2O is not constrained) at $-10^\circ C$ [13, 49]. Consequently, due to these differences in permeability, the mixing ratios of O_2 and Ar are likely to decrease, while the mixing ratios of N_2 , CO_2 , and CH_4 may increase in ice bubbles. However, the increase of CO_2 mixing ratio by the gas diffusion is not likely more than that of N_2 due to the similar permeation coefficients (1.39 vs. $1.31 \times 10^{-19} \text{ m}^2/\text{s} \cdot \text{MPa}$).

5.2.1 | Carbon Dioxide, CO_2

The observed high CO_2 mixing ratios in the ice wedges may be caused by biological respiration, which is a process that consumes O_2 and produces CO_2 . The stable carbon isotope ratio of CO_2 can provide valuable information regarding the source of CO_2 entrapped in ice wedges [50]. The isotopic ratios (see Section 4.5) indicate that the CO_2 found in Batagay ice wedges mostly originated from microbial oxidation of sediment organics [51]. However, the mean values of $\delta^{13}C-CO_2$ were slightly greater than those of sediments in the Batagay ice wedges. This discrepancy could be attributed to mixing with atmospheric CO_2 , which tends to increase the $\delta^{13}C-CO_2$ values. However, the observed CO_2 mixing ratios were approximately 160 times greater than the atmospheric values from LGM [52]. Meanwhile, the weathering of carbonate minerals, which typically indicate a $\delta^{13}C$ value of approximately 0‰, can increase carbon isotope values [53]. Based on mass balance calculation, we estimate that the CO_2 production from the carbonate minerals can explain less than 12% of the CO_2 in the bubbles. For instance, if we take the fraction of CO_2 originating from carbonate as “f,” the mass balance equation ($0‰ \times f + -25.8‰ \times (1 - f) = -22.8‰$) yields solution for “f” at 0.12. Hence, we conclude that most of the CO_2 in Batagay ice wedges originated from biological respiration.

5.2.2 | Methane, CH_4

There are both abiotic and biotic CH_4 production processes [54]. Most abiotic processes require suitable thermal conditions ($300^\circ C-400^\circ C$) instead of subfreezing conditions [54]. Despite the recent exposure of the Batagay megaslump due to anthropogenic disturbance, the permafrost and ice wedges in the area remain in a stable state, characterized by low temperatures. Furthermore, the undisturbed foliations observed in the ice wedges indicate that they were not affected by geothermal and physical activity during or after their formation. Hence, we can exclude the thermogenic process as the primary source of CH_4 in the Batagay ice wedges.

The carbon isotope ratios of methane can provide valuable information about methane production processes in permafrost regions [55–57]. Courtin et al. [58], identified certain methanogenic archaea in the Batagay ice complex units (UIC, LIC), indicating the possibility of biogenic processes occurring in ice wedges. According to Whiticar et al. [55], the $\delta^{13}C-CH_4$ values of the LIC ($-47.3‰$, $-48.9‰$) are indicative of bacterial origin ($< -45‰$), whereas the $\delta^{13}C$ value of the UIC ($-36.7‰$) indicates thermogenic origin ($-20‰$ to $-50‰$) [55]. However, as we have already excluded the possibility of thermogenic CH_4 production, the relatively enriched $\delta^{13}C-CH_4$ value from the UIC could be attributable to isotopic fractionation during its exchange with

and transformation to CO₂. Whiticar [55] suggested using the isotopic separation factor (ϵ_c), where $\epsilon_c = \delta^{13}\text{C-CO}_2 - \delta^{13}\text{C-CH}_4$, to infer the methane production or consumption process. In this study, the LIC and UIC exhibited ϵ_c values of 24.5 and 12.9, respectively, which were within the range for methane oxidation [55]. Furthermore, methane-oxidizing bacteria have been reported to alter the carbon isotope composition of CH₄ [59]. These bacteria preferentially consume ¹²C, thus yielding values of lighter isotopes in the resulting CO₂, whereas the remaining CH₄ becomes enriched in heavier isotopes. This can potentially result in the misinterpretation of biogenic CH₄ signatures as natural gas deposits or having thermogenic origins. Earlier studies have shown a correlation between anaerobic methane oxidation with reductions in nitrate and sulfate, suggesting that methane oxidation can occur even in anaerobic conditions [60, 61]. Therefore, it is plausible that methane in ice wedges may have undergone such processes, potentially impacting its isotopic composition.

5.2.3 | Nitrous Oxide, N₂O

Compared with atmospheric levels in the Middle and Late Pleistocene and Holocene (200–300 ppb) [45], the elevated N₂O mixing ratios in the Batagay ice wedges may be attributed to N₂O production in the ice wedges.

Microbial nitrification and denitrification processes were considered for the N₂O production pathways in permafrost-affected sediments [62]. In the case of Batagay, both nitrification and denitrification processes can be potential sources of N₂O due to the heterogeneous distribution of oxygen gas in the Batagay ice wedges [63]. Multiple studies have demonstrated that N₂O production can remain active in seasonally frozen soils, even at subzero temperatures, thus indicating that the sediments within ice wedges can produce N₂O within the ice wedge system [11, 62]. Nitrification is a strictly aerobic condition that requires O₂ as an electron acceptor for a series of oxidative reactions that convert NH₄⁺ to NO₂⁻ and NO₃⁻. This process is facilitated by ammonia-oxidizing archaea and bacteria, which produce N₂O as a byproduct. The low O₂ mixing ratios in the ice complexes from Batagay (<5%) suggest that nitrification could have dominated in the initial stages of ice wedge formation but may not be the dominant source of N₂O production in the later stage [63, 64]. However, significant N₂O emissions through nitrification have been observed under low-oxygen conditions in other studies [65]; therefore, we cannot completely preclude the significant contribution of nitrification in a later stage.

In denitrification, both NO₂⁻ and NO₃⁻ act as electron acceptors for denitrifiers in an anaerobic respiration pathway, thus resulting in their reduction to N₂, with NO and N₂O as gas intermediates [66]. Soil incubation studies demonstrated that N₂O can be produced by denitrification and nitrifier-denitrification under low oxygen condition [66, 67]. Under completely anoxic conditions, N₂O is predominantly produced through denitrification [66]. Hence, it can be expected that denitrification and nitrifier-denitrification are dominant processes under low oxygen condition periods.

A relationship between the N₂O and CH₄ mixing ratios was observed in Batagay ice wedges. In the UIC, low CH₄ was

accompanied by very high N₂O mixing ratios, and vice versa for the LIC (Figure 6b). This pattern is consistent with previous findings pertaining to other ice wedges from Siberia, where the distribution of CH₄ and N₂O mixing ratios showed distinct characteristics (Figure 6b) [13, 15]. This “exclusive relationship” may be explained by the inhibitory effect of N-containing compounds (NO₃⁻, NO₂⁻, NO, and N₂O) on methanogenesis. Several studies have reported a decrease in methanogenic bacterial activity in the presence of N₂O [15, 68]. Hence, the low N₂O mixing ratios and relatively high CH₄ mixing ratios in the LIC is attributable to its low potential to generate N-containing compounds, including N₂O, which subsequently promotes more active methanogenesis.

Meanwhile, the average N₂O mixing ratios in the UIC were considerably higher than those in the LIC. In order to elucidate this phenomenon, we examined two perspectives related to vegetation and microorganisms. Vegetation can affect environmental factors, such as soil pH and nutrient cycling. Therefore, the differences in vegetation between the UIC and LIC at the time of formation provide insights into the variation in biogeochemical factors for N₂O production. Courtin et al. [58], suggest that LIC reflects an interglacial ecosystem which has open forests with grassland, and UIC reflects a glacial ecosystem with herb communities dominating the vegetation. Although the reference shows that there are environmental differences between the UIC and LIC, our analysis of sediment characteristics, including sediment C/N ratios and $\delta^{13}\text{C}$ values (Table 1), in both ice complex units exhibit no significant differences. On the other hand, microbial activities and specific enzymes can play a crucial role in N₂O production. Previous studies showed the existence of different prokaryotic communities in the sediments of upper and lower units of the Batagay megaslump, with higher numbers of ammonia-oxidizing archaea (AOA) in the UIC sediments than in the LIC sediments [58]. Numerous *Nitrososphaeraceae* and *Nitrosopumilaceae* families were detected, which constitute AOA families and are known to be key contributors to N₂O emissions in Arctic soils [69, 70]. These differences in the archaeal community may explain the variations in N₂O levels between the UIC and LIC ice wedges. On the other hand, the different ages of the LIC and the UIC can influence N₂O mixing ratios as well. If denitrification activity is the same in both units, the LIC would reduce more N₂O and produce more N₂ than the UIC due to having more reaction time. However, as the availability of NO₃⁻ is crucial in denitrification and AOA plays a significant role in creating NO₃⁻, the low abundance of AOA in the LIC reduces the likelihood of NO₃⁻ supply for N₂O production. Hence, age differences might not significantly affect N₂O mixing ratios. Although a specific examination of the sediment microbiome trapped inside the ice wedges was not conducted in this study, insights from the surrounding sediments can provide some understanding regarding processes occurring in the ice wedges.

In some laboratory experiments, abiotic processes for N₂O production have been reported. These include chemo-denitrification, which involves the chemical reduction of NO₃⁻ through reaction with Fe²⁺, as well as the oxidation of NH₂OH in soils [71]. However, such natural observations are relatively scarce. There was a notable instance of chemo-denitrification with Fe²⁺ reported in the brine of ice-sealed Vida Lake, Antarctica [72]. To investigate the possibility, we analyzed total

Fe concentration and obtained values of 0.386 ± 0.216 mg/L and 0.048 ± 0.068 mg/L for the LIC and UIC, respectively (Table S2). These Fe concentrations are comparable to those found in the pore water and peat ice of the Western Siberian Lowland, which are 0.68 and 2.05 mg/L, respectively [73]. However, they are two orders of magnitude smaller than the reported Fe^{2+} concentration in the brine of Vida Lake, which was 17.195 ± 1.262 mg/L for Fe^{2+} [73, 74]. Further investigation is necessary to explore the possibility of these abiotic reactions, including the examination of proton concentrations (pH). Protons may have an impact on the abiotic reactions [75], particularly within the ice veins and thin films around sediment particles. These areas exhibit distinct geochemical conditions from bulk environment, potentially due to freeze-concentration effects [76–78].

6 | Conclusion

The Batagay ice complex units have provided valuable biogeochemical information pertaining to ground ice in the Yana Uplands since the Middle Pleistocene. Our observations indicate that the ice wedges were formed by the compaction of dry snow and/or hoar frost, as indicated by the N_2/Ar ratios and bubble shapes. The higher mixing ratios of GHGs in the Batagay ice wedges compared with those in the Pleistocene atmosphere implied a substantial contribution from microbial activity in the ice wedges. The carbon stable isotope values suggested that CO_2 and CH_4 originated primarily from microbial sources. The high level of N_2O compared with the preindustrial atmosphere can be attributable to microbial activity instead of abiotic factors. Notably, the UIC and the LIC units show differences in terms of N_2O mixing ratios, which is likely due to the UIC having more of specific ammonia-oxidizing archaeal families instead of environmental or climatic differences. This suggests that biogeochemical factors in ice wedges can vary even within the same location, thus highlighting that GHG formation in ice wedges is not solely controlled by physiochemical conditions. This study provides insights into the complex relationships between microbial activity and biogeochemical conditions for GHG formation and storage in permafrost ice wedges.

Acknowledgments

This study is supported by National Research Foundation of Korea (2020M1A5A1110607; 2018R1A5A1024958) grant to JA and the Leverhulme Trust Research Project Grant (RPG-2020-334) to TO. We also would like to thank all members of the Russian-German expedition to the Batagay megaslump in spring 2019 for their support during fieldwork. We thank the editor and two anonymous reviewers for their valuable comments during the review process.

Data Availability Statement

The data that support the findings of this study are available from the corresponding author upon reasonable request.

References

1. G. Hugelius, J. Strauss, S. Zubrzycki, et al., “Estimated Stocks of Circumpolar Permafrost Carbon With Quantified Uncertainty Ranges and Identified Data Gaps,” *Biogeosciences* 11, no. 23 (2014): 6573–6593, <https://doi.org/10.5194/bg-11-6573-2014>.

2. V. G. Salmon, C. Schädel, R. Bracho, et al., “Adding Depth to Our Understanding of Nitrogen Dynamics in Permafrost Soils,” *Journal of Geophysical Research – Biogeosciences* 123, no. 8 (2018): 2497–2512, <https://doi.org/10.1029/2018JG004518>.
3. A. K. Liljedahl, J. Boike, R. P. Daanen, et al., “Pan-Arctic Ice-Wedge Degradation in Warming Permafrost and Its Influence on Tundra Hydrology,” *Nature Geoscience* 9, no. 4 (2016): 312–318, <https://doi.org/10.1038/ngeo2674>.
4. Y. Shur, D. Fortier, M. T. Jorgenson, et al., “Yedoma Permafrost Genesis: Over 150 Years of Mystery and Controversy,” *Frontiers in Earth Science* 9, no. January (2022): 1–21, <https://doi.org/10.3389/feart.2021.757891>.
5. L. Schirrmeister, D. Froese, V. Tumskey, G. Grosse, and S. Wetterich, *Yedoma: Late Pleistocene Ice-Rich Syngenetic Permafrost of Beringia*, vol. 3, 2nd ed., (Amsterdam: Elsevier B.V., 2013), <https://doi.org/10.1016/B978-0-444-53643-3.00106-0>.
6. H. Pörtner, D. Roberts, and V. Masson-Delmotte, “Summary for Policymakers: Climate Change 2022_ Impacts, Adaptation and Vulnerability_Working Group II Contribution to the Sixth Assessment Report of the Intergovernmental Panel on Climate Change,” (2022), <https://doi.org/10.1017/9781009325844.Front>.
7. T. Opel, H. Meyer, S. Wetterich, T. Laepple, A. Dereviagin, and J. Murton, “Ice Wedges as Archives of Winter Paleoclimate: A Review,” *Permafrost and Periglacial Processes* 29, no. 3 (2018): 199–209, <https://doi.org/10.1002/ppp.1980>.
8. M. St-Jean, B. Lauriol, I. D. Clark, D. Lacelle, and C. Zdanowicz, “Investigation of Ice-Wedge Infilling Processes Using Stable Oxygen and Hydrogen Isotopes, Crystallography and Occluded Gases (O_2 , N_2 , Ar),” *Permafrost and Periglacial Processes* 22, no. 1 (2011): 49–64, <https://doi.org/10.1002/ppp.680>.
9. A. Brouchkov and M. Fukuda, “Preliminary Measurements on Methane Content in Permafrost, Central Yakutia, and Some Experimental Data,” *Permafrost and Periglacial Processes* 13, no. 3 (2002): 187–197, <https://doi.org/10.1002/ppp.422>.
10. R. Teepe, R. Brumme, and F. Beese, “Nitrous Oxide Emissions From Soil During Freezing and Thawing Periods,” *Soil Biology and Biochemistry* 33, no. 9 (2001): 1269–1275, [https://doi.org/10.1016/S0038-0717\(01\)00084-0](https://doi.org/10.1016/S0038-0717(01)00084-0).
11. M. G. Öquist, M. Nilsson, F. Sörensson, et al., “Nitrous Oxide Production in a Forest Soil at Low Temperatures - Processes and Environmental Controls,” *FEMS Microbiology Ecology* 49, no. 3 (2004): 371–378, <https://doi.org/10.1016/j.femsec.2004.04.006>.
12. S. Wetterich, H. Meyer, M. Fritz, et al., “Northeast Siberian Permafrost Ice-Wedge Stable Isotopes Depict Pronounced Last Glacial Maximum Winter Cooling,” *Geophysical Research Letters* 48, no. 7 (2021): e2020GL092087, <https://doi.org/10.1029/2020GL092087>.
13. K. Kim, J. W. Yang, H. Yoon, et al., “Greenhouse Gas Formation in Ice Wedges at Cyuie, Central Yakutia,” *Permafrost and Periglacial Processes* 30, no. 1 (2019): 48–57, <https://doi.org/10.1002/ppp.1994>.
14. T. Boereboom, D. Samyn, H. Meyer, and J.-L. Tison, “Stable Isotope and Gas Properties of Two Climatically Contrasting (Pleistocene and Holocene) Ice Wedges From Cape Mamontov Klyk, Laptev Sea, Northern Siberia,” *The Cryosphere* 7, no. 1 (2013): 31–46, <https://doi.org/10.5194/tc-7-31-2013>.
15. J. Yang, J. Ahn, G. Iwahana, et al., “Origin of CO_2 , CH_4 , and N_2O Trapped in Ice Wedges in Central Yakutia and Their Relationship,” *Permafrost and Periglacial Processes* 34 (2023): 122–141, <https://doi.org/10.1002/ppp.2176>.
16. K. Ashastina, L. Schirrmeister, M. Fuchs, and F. Kienast, “Palaeoclimate Characteristics in Interior Siberia of MIS 6-2: First Insights From the Batagay Permafrost Mega-Thaw Slump in the Yana Highlands,” *Climate of the Past* 13, no. 7 (2017): 795–818, <https://doi.org/10.5194/cp-13-795-2017>.

17. J. Murton, T. Opel, S. Wetterich, et al., "Batagay Megalump: A Review of the Permafrost Deposits, Quaternary Environmental History, and Recent Development," *Permafrost and Periglacial Processes* 34 (2023): 399–416, <https://doi.org/10.1002/ppp.2194>.
18. J. B. Murton, T. Opel, P. Toms, et al., "A Multimethod Dating Study of Ancient Permafrost, Batagay Megalump, East Siberia," *Quaternary Research* 105 (2022): 1–22, <https://doi.org/10.1017/qua.2021.27>.
19. H. French and Y. Shur, "The Principles of Cryostratigraphy," *Earth-Science Reviews* 101, no. 3–4 (2010): 190–206, <https://doi.org/10.1016/j.earscirev.2010.04.002>.
20. R. C. Wilhelm, K. J. Radtke, N. C. S. Mykityczuk, C. W. Greer, and L. G. Whyte, "Life at the Wedge: The Activity and Diversity of Arctic Ice Wedge Microbial Communities," *Astrobiology* 12, no. 4 (2012): 347–360, <https://doi.org/10.1089/ast.2011.0730>.
21. A. I. Kizyakov, S. Wetterich, F. Günther, et al., "Landforms and Degradation Pattern of the Batagay Thaw Slump, Northeastern Siberia," *Geomorphology* 420, no. October 2022 (2023): 108501, <https://doi.org/10.1016/j.geomorph.2022.108501>.
22. T. Opel, J. B. Murton, S. Wetterich, et al., "Past Climate and Continentality Inferred From Ice Wedges at Batagay Megalump in the Northern Hemisphere's Most Continental Region, Yana Highlands, Interior Yakutia," *Climate of the Past* 15, no. 4 (2019): 1443–1461, <https://doi.org/10.5194/cp-15-1443-2019>.
23. J. B. Murton, M. E. Edwards, A. V. Lozhkin, et al., "Preliminary Paleoenvironmental Analysis of Permafrost Deposits at Batagaika Megalump, Yana Uplands, Northeast Siberia," *Quaternary Research* 87 (2017): 314–330, <https://doi.org/10.1017/qua.2016.15>.
24. L. L. Jongejans, T. Opel, J. Courtin, et al., "Batagay Spring 2019," (2019).
25. Y. Ryu, J. Ahn, and J. W. Yang, "High-Precision Measurement of N₂O Concentration in Ice Cores," *Environmental Science & Technology* 52, no. 2 (2018): 731–738, <https://doi.org/10.1021/acs.est.7b05250>.
26. J. W. Yang, J. Ahn, G. Iwahana, S. Han, K. Kim, and A. Fedorov, "Brief Communication: The Reliability of Gas Extraction Techniques for Analysing CH₄ and N₂O Compositions in Gas Trapped in Permafrost Ice Wedges," *The Cryosphere* 14, no. 4 (2020): 1311–1324, <https://doi.org/10.5194/tc-14-1311-2020>.
27. H. D. Holland, *The Chemical Evolution of the Atmosphere and Oceans* (Princeton, NJ: Princeton University Press, 1984), <https://doi.org/10.2307/j.ctv15r58kg>.
28. W. Dansgaard, "Stable Isotopes in Precipitation," *Tellus* 16, no. 4 (1964): 436, <https://doi.org/10.3402/tellusa.v16i4.8993>.
29. A. J. Midwood and T. W. Boutton, "Soil Carbonate Decomposition by Acid Has Little Effect on $\delta^{13}\text{C}$ of Organic Matter," *Soil Biology and Biochemistry* 30, no. 10–11 (1998): 1301–1307, [https://doi.org/10.1016/S0038-0717\(98\)00030-3](https://doi.org/10.1016/S0038-0717(98)00030-3).
30. U. Tsunogai, F. Nakagawa, F. Nakagawa, and Y. Hachisu, "Stable Carbon and Oxygen Isotopic Analysis of Carbon Monoxide in Natural Waters," *Rapid Communications in Mass Spectrometry* 14, no. 16 (2000): 1507–1512, [https://doi.org/10.1002/1097-0231\(20000830\)14:16<1507::AID-RCM56>3.0.CO;2-E](https://doi.org/10.1002/1097-0231(20000830)14:16<1507::AID-RCM56>3.0.CO;2-E).
31. S. Kawagucci, U. Tsunogai, S. Kudo, et al., "An Analytical System for Determining $\delta^{17}\text{O}$ in CO₂ Using Continuous Flow-Isotope Ratio MS," *Analytical Chemistry* 77, no. 14 (2005): 4509–4514, <https://doi.org/10.1021/ac050266u>.
32. A. Hirota, U. Tsunogai, D. D. Komatsu, and F. Nakagawa, "Simultaneous Determination of $\delta^{15}\text{N}$ and $\delta^{18}\text{O}$ of N₂O and $\delta^{13}\text{C}$ of CH₄ in Nanomolar Quantities From a Single Water Sample," *Rapid Communications in Mass Spectrometry* 24, no. 7 (2010): 1085–1092, <https://doi.org/10.1002/rcm.4483>.
33. T. S. Papina, N. S. Malygina, A. N. Eirikh, A. A. Galanin, and M. N. Zheleznyak, "Isotopic Composition and Sources of Atmospheric Precipitation in Central Yakutia," *Earth's Cryosphere* 21, no. 2 (2017): 60–69, [https://doi.org/10.21782/KZ1560-7496-2017-2\(60-69\)](https://doi.org/10.21782/KZ1560-7496-2017-2(60-69)).
34. M. Rubino, D. M. Etheridge, C. M. Trudinger, et al., "A Revised 1000 Year Atmospheric $\delta^{13}\text{C}$ -CO₂ Record From Law Dome and South Pole, Antarctica," *Journal of Geophysical Research – Atmospheres* 118, no. 15 (2013): 8482–8499, <https://doi.org/10.1002/jgrd.50668>.
35. T. Ikeda-Fukazawa, K. Kawamura, and T. Hondoh, "Mechanism of Molecular Diffusion in Ice Crystals," *Molecular Simulation* 30, no. 13–15 (2004): 973–979, <https://doi.org/10.1080/08927020410001709307>.
36. T. Ikeda-Fukazawa, S. Horikawa, T. Hondoh, and K. Kawamura, "Molecular Dynamics Studies of Molecular Diffusion in Ice Ih," *The Journal of Chemical Physics* 117, no. 8 (2002): 3886–3896, <https://doi.org/10.1063/1.1495844>.
37. T. Ikeda-Fukazawa, K. Fukumizu, K. Kawamura, S. Aoki, T. Nakazawa, and T. Hondoh, "Effects of Molecular Diffusion on Trapped Gas Composition in Polar Ice Cores," *Earth and Planetary Science Letters* 229, no. 3–4 (2005): 183–192, <https://doi.org/10.1016/j.epsl.2004.11.011>.
38. Y. S. Yi, Y. Han, K. D. Kwon, S. K. Lee, and S. D. Hur, "Molecular Mechanism of Gas Diffusion in Ice-Ih," *ACS Earth and Space Chemistry* 5, no. 11 (2021): 3258–3267, <https://doi.org/10.1021/acsearthspacechem.1c00308>.
39. I. Oyabu, K. Kawamura, T. Uchida, et al., "Fractionation of O₂/N₂ and Ar/N₂ in the Antarctic Ice Sheet During Bubble Formation and Bubble–Clathrate Hydrate Transition From Precise Gas Measurements of the Dome Fuji Ice Core," *The Cryosphere* 15, no. 12 (2021): 5529–5555, <https://doi.org/10.5194/tc-2021-147>.
40. H. Meyer, A. Dereviagin, C. Siegert, L. Schirmermeister, and H. W. Hubberten, "Palaeoclimate Reconstruction on Big Lyakhovskiy Island, North Siberia - Hydrogen and Oxygen Isotopes in Ice Wedges," *Permafrost and Periglacial Processes* 13, no. 2 (2002): 91–105, <https://doi.org/10.1002/ppp.416>.
41. T. Opel, A. Y. Dereviagin, H. Meyer, L. Schirmermeister, and S. Wetterich, "Palaeoclimatic Information From Stable Water Isotopes of Holocene Ice Wedges on the Dmitrii Laptev Strait, Northeast Siberia, Russia," *Permafrost and Periglacial Processes* 22, no. 1 (2011): 84–100, <https://doi.org/10.1002/ppp.667>.
42. J.-W. Yang, J. Ahn, E. Brook, and Y. Ryu, "Atmospheric Methane Control Mechanisms During the Early Holocene," *Climate of the Past Discussions* 4 (2017): 1–22, <https://doi.org/10.5194/cp-2016-75>.
43. D. Lüthi, M. Le Floch, B. Bereiter, et al., "High-Resolution Carbon Dioxide Concentration Record 650,000–800,000 Years Before Present," *Nature* 453, no. 7193 (2008): 379–382, <https://doi.org/10.1038/nature06949>.
44. L. Loulergue, A. Schilt, R. Spahni, et al., "Orbital and Millennial-Scale Features of Atmospheric CH₄ Over the Past 800,000 Years," *Nature* 453, no. 7193 (2008): 383–386, <https://doi.org/10.1038/nature06950>.
45. A. Schilt, M. Baumgartner, T. Blunier, et al., "Glacial-Interglacial and Millennial-Scale Variations in the Atmospheric Nitrous Oxide Concentration During the Last 800,000 Years," *Quaternary Science Reviews* 29, no. 1–2 (2010): 182–192, <https://doi.org/10.1016/j.quascirev.2009.03.011>.
46. M. P. Nikrad, L. J. Kerkhof, and M. M. Häggblom, "The Subzero Microbiome: Microbial Activity in Frozen and Thawing Soils," *FEMS Microbiology Ecology* 92, no. 6 (2016): 1–16, <https://doi.org/10.1093/femsec/fiw081>.
47. T. Katayama, M. Tanaka, J. Moriizumi, et al., "Phylogenetic Analysis of Bacteria Preserved in a Permafrost Ice Wedge for 25,000 Years," *Applied and Environmental Microbiology* 73, no. 7 (2007): 2360–2363, <https://doi.org/10.1128/AEM.01715-06>.
48. C. Bakermans, A. I. Tsapin, V. Souza-Egipsy, D. A. Gilichinsky, and K. H. Nealson, "Reproduction and Metabolism at –10°C of Bacteria Isolated From Siberian Permafrost," *Environmental Microbiology* 5, no. 4 (2003): 321–326, <https://doi.org/10.1046/j.1462-2920.2003.00419.x>.
49. J. Ahn, M. Headly, M. Wahlen, E. J. Brook, P. A. Mayewski, and K. C. Taylor, "CO₂ Diffusion in Polar Ice: Observations From

- Naturally Formed CO₂ Spikes in the Siple Dome (Antarctica) Ice Core,” *Journal of Glaciology* 54, no. 187 (2008): 685–695, <https://doi.org/10.3189/002214308786570764>.
50. M. S. Lachniet, D. E. Lawson, and A. R. Sloat, “Revised ¹⁴C Dating of Ice Wedge Growth in Interior Alaska (USA) to MIS 2 Reveals Cold Paleoclimate and Carbon Recycling in Ancient Permafrost Terrain,” *Quaternary Research* 78, no. 2 (2012): 217–225, <https://doi.org/10.1016/j.yqres.2012.05.007>.
51. M. H. O’Leary, “Carbon Isotope Fractionation in Plants,” *Phytochemistry* 20, no. 4 (1981): 553–567, [https://doi.org/10.1016/0031-9422\(81\)85134-5](https://doi.org/10.1016/0031-9422(81)85134-5).
52. B. Hönisch, N. G. Hemming, D. Archer, M. Siddall, and J. F. McManus, “Atmospheric Carbon Dioxide Concentration Across the mid-Pleistocene Transition,” *Science* 324, no. 5934 (2009): 1551–1554, <https://doi.org/10.1126/science.1171477>.
53. L. S. Land, “The Isotopic and Trace Element Geochemistry of Dolomite: The State of the Art,” in *Concepts Model Dolomitization*, eds. D. H. Zenger, J. B. Dunham, and R. L. Ethington (Broken Arrow, OK: Society for Sedimentary Geology, 1980), 87–110, <https://doi.org/10.2110/pec.80.28.0087>.
54. G. Etiope and B. Sherwood Lollar, “Abiotic Methane on Earth,” *Reviews of Geophysics* 51, no. 2 (2013): 276–299, <https://doi.org/10.1002/rog.20011>.
55. M. J. Whiticar, “Carbon and Hydrogen Isotope Systematics of Bacterial Formation and Oxidation of Methane,” *Chemical Geology* 161, no. 1 (1999): 291–314, [https://doi.org/10.1016/S0009-2541\(99\)00092-3](https://doi.org/10.1016/S0009-2541(99)00092-3).
56. E. Rivkina, V. Shcherbakova, K. Laurinavichius, et al., “Biogeochemistry of Methane and Methanogenic Archaea in Permafrost,” *FEMS Microbiology Ecology* 61, no. 1 (2007): 1–15, <https://doi.org/10.1111/j.1574-6941.2007.00315.x>.
57. L. Høj, R. A. Olsen, and V. L. Torsvik, “Archaeal Communities in High Arctic Wetlands at Spitsbergen, Norway (78°N) as Characterized by 16S rRNA Gene Fingerprinting,” *FEMS Microbiology Ecology* 53, no. 1 (2005): 89–101, <https://doi.org/10.1016/j.femsec.2005.01.004>.
58. J. Courtin, A. Perfumo, A. A. Andreev, et al., “Pleistocene Glacial and Interglacial Ecosystems Inferred From Ancient DNA Analyses of Permafrost Sediments From Batagay Megalump, East Siberia,” *Environmental DNA* 4 (2022): 1265–1283, <https://doi.org/10.1002/edn3.336>.
59. J. F. Barker and P. Fritz, “Carbon Isotope Fractionation During Microbial Methane Oxidation,” *Nature* 293, no. September (1981): 289–291.
60. S. E. McGlynn, G. L. Chadwick, C. P. Kempes, and V. J. Orphan, “Single Cell Activity Reveals Direct Electron Transfer in Methanotrophic Consortia,” *Nature* 526, no. 7574 (2015): 531–535, <https://doi.org/10.1038/nature15512>.
61. M. F. Haroon, S. Hu, Y. Shi, et al., “Anaerobic Oxidation of Methane Coupled to Nitrate Reduction in a Novel Archaeal Lineage,” *Nature* 500, no. 7464 (2013): 567–570, <https://doi.org/10.1038/nature12375>.
62. C. Voigt, M. E. Marushchak, B. W. Abbott, et al., “Nitrous Oxide Emissions From Permafrost-Affected Soils,” *Nature Reviews Earth and Environment* 1, no. 8 (2020): 420–434, <https://doi.org/10.1038/s43017-020-0063-9>.
63. J. M. Tiedje, “Ecology of Denitrification and Dissimilatory Nitrate Reduction to Ammonium,” in *Biology of Anaerobic Microorganisms*, (New York, NY: John Wiley & Sons, 1988), 179–244.
64. K. Khalil, B. Mary, and P. Renault, “Nitrous Oxide Production by Nitrification and Denitrification in Soil Aggregates as Affected by O₂ Concentration,” *Soil Biology and Biochemistry* 36, no. 4 (2004): 687–699, <https://doi.org/10.1016/j.soilbio.2004.01.004>.
65. E. J. Bateman and E. M. Baggs, “Contributions of Nitrification and Denitrification to N₂O Emissions From Soils at Different Water-Filled Pore Space,” *Biology and Fertility of Soils* 41, no. 6 (2005): 379–388, <https://doi.org/10.1007/s00374-005-0858-3>.
66. X. Zhu, M. Burger, T. A. Doane, and W. R. Horwath, “Ammonia Oxidation Pathways and Nitrifier Denitrification Are Significant Sources of N₂O and NO Under Low Oxygen Availability,” *Proceedings of the National Academy of Sciences of the United States of America* 110, no. 16 (2013): 6328–6333, <https://doi.org/10.1073/pnas.1219931110>.
67. N. E. Ostrom, R. Sutka, P. H. Ostrom, et al., “Isotopologue Data Reveal Bacterial Denitrification as the Primary Source of N₂O During a High Flux Event Following Cultivation of a Native Temperate Grassland,” *Soil Biology and Biochemistry* 42, no. 3 (2010): 499–506, <https://doi.org/10.1016/j.soilbio.2009.12.003>.
68. H. D. Klüber and R. Conrad, “Inhibitory Effects of Nitrate, Nitrite, NO and N₂O on Methanogenesis by *Methanosarcina barkeri* and *Methanobacterium bryantii*,” *FEMS Microbiology Ecology* 25, no. 4 (1998): 331–339, [https://doi.org/10.1016/S0168-6496\(97\)00102-5](https://doi.org/10.1016/S0168-6496(97)00102-5).
69. J. I. Prosser, L. Hink, C. Gubry-Rangin, and G. W. Nicol, “Nitrous Oxide Production by Ammonia Oxidizers: Physiological Diversity, Niche Differentiation and Potential Mitigation Strategies,” *Global Change Biology* 26, no. 1 (2020): 103–118, <https://doi.org/10.1111/gcb.14877>.
70. R. J. E. Alves, M. Kerou, A. Zappe, et al., “Ammonia Oxidation by the Arctic Terrestrial Thaumarchaeote Candidatus Nitrosocosmicus Arcticus Is Stimulated by Increasing Temperatures,” *Frontiers in Microbiology* 10 (2019): 1571, <https://doi.org/10.3389/fmicb.2019.01571>.
71. J. M. Bremner, A. M. Blackmer, and S. A. Waring, “Formation of Nitrous Oxide and Dinitrogen by Chemical Decomposition of Hydroxylamine in Soils,” *Soil Biology and Biochemistry* 12, no. 3 (1980): 263–269, [https://doi.org/10.1016/0038-0717\(80\)90072-3](https://doi.org/10.1016/0038-0717(80)90072-3).
72. N. E. Ostrom, H. Gandhi, G. Trubl, and A. E. Murray, “Chemodenitrification in the Cryoecosystem of Lake Vida, Victoria Valley, Antarctica,” *Geobiology* 14, no. 6 (2016): 575–587, <https://doi.org/10.1111/gbi.12190>.
73. A. G. Lim, S. V. Loiko, D. M. Kuzmina, et al., “Dispersed Ground Ice of Permafrost Peatlands: Potential Unaccounted Carbon, Nutrient and Metal Sources,” *Chemosphere* 266 (2021): 128953, <https://doi.org/10.1016/j.chemosphere.2020.128953>.
74. A. E. Murray, F. Kenig, C. H. Fritsen, et al., “Microbial Life at –13°C in the Brine of an Ice-Sealed Antarctic Lake,” *Proceedings of the National Academy of Sciences of the United States of America* 109, no. 50 (2012): 20626–20631, <https://doi.org/10.1073/pnas.1208607109>.
75. L. I. Gordon and J. H. Butler, “Rates of Nitrous Oxide Production in the Oxidation of Hydroxylamine by Iron (III),” *Inorganic Chemistry* 25, no. 25 (1986): 4573–4577, <https://doi.org/10.1021/ic00245a024>.
76. P. Kolhe, E. Amend, and S. K. Singh, “Impact of Freezing on pH of Buffered Solutions and Consequences for Monoclonal Antibody Aggregation,” *Biotechnology Progress* 26, no. 3 (2010): 727–733, <https://doi.org/10.1002/btpr.377>.
77. K. Kim, J. Ju, B. Kim, et al., “Nitrite-Induced Activation of Iodate into Molecular Iodine in Frozen Solution,” *Environmental Science & Technology* 53, no. 9 (2019): 4892–4900, <https://doi.org/10.1021/acs.est.8b06638>.
78. N. T. H. le, J. Ju, B. Kim, et al., “Freezing-Enhanced Non-radical Oxidation of Organic Pollutants by Peroxymonosulfate,” *Chemical Engineering Journal* 388, no. January (2020): 124226, <https://doi.org/10.1016/j.cej.2020.124226>.

Supporting Information

Additional supporting information can be found online in the Supporting Information section.